Electronic Supplementary Material (ESI) for Physical Chemistry Chemical Physics.

Monitoring Aromatic Ring-Currents in Mg-porphyrin by Time-Resolved Circular Dichroism

Yeonsig Nam[1,2], Jérémy R. Rouxel[1], Jin Yong Lee[2], and Shaul Mukamel[1]

[1]Department of Chemistry, University of California, Irvine, California 92697-2025, USA
[2]Department of Chemistry, Sungkyunkwan University, Suwon, South Korea, 16419

October 27, 2020

Contents

1 Details of the time-resolved circular dichroism signal calculation **2**

2 Quantum simulation results **7**

3 Time-dependent density matrix elements and Average transition current density **8**

1 Details of the time-resolved circular dichroism signal calculation

We start with the minimal coupling Hamiltonian, retaining only the current density term:

$$H_{\text{int}} = -\int \mathrm{d}\boldsymbol{r}\boldsymbol{j}(\boldsymbol{r}) \cdot \boldsymbol{A}(\boldsymbol{r}, t) \tag{1}$$

where $\boldsymbol{j}(\boldsymbol{r})$ is transition current density and $\boldsymbol{A}(\boldsymbol{r}, t)$ is a vector potential of incoming pulse. The heterodyne-detected signal is defined as the change of the number of photons in a given time,

$$S(\Gamma) = \int \mathrm{d}t \langle \dot{N}_s \rangle \tag{2}$$

where, Γ indicates the set of parameters, i.e. incoming pulses central frequencies, durations, etc.

$$\dot{N}_s = \frac{i}{\hbar}[H_{\text{int}}, N_s] = -\frac{i}{\hbar}[\int \mathrm{d}\boldsymbol{r} j(\boldsymbol{r}) \boldsymbol{A}(\boldsymbol{r}, t), a_s^\dagger a_s] \tag{3}$$

The vector potential $\boldsymbol{A}(\boldsymbol{r}, t)$ can be expressed as the following:

$$\boldsymbol{A}(\boldsymbol{r}, t) = \sqrt{\frac{\hbar}{2\epsilon_0 \omega_S \Omega}} (a_s \boldsymbol{\varepsilon} e^{i(\boldsymbol{k}_s \cdot \boldsymbol{r} - \omega_s t)} + a_s^\dagger \boldsymbol{\varepsilon}^* e^{-i(\boldsymbol{k}_s \cdot \boldsymbol{r} - \omega_s t)}) \tag{4}$$

where $\boldsymbol{\varepsilon}$ is the electric field polarization vectors. Hence, it gives

$$\dot{N}_s = -\frac{i}{\hbar} \int \mathrm{d}\boldsymbol{r} j(\boldsymbol{r}) \cdot [\boldsymbol{A}(\boldsymbol{r}, t), a_s^\dagger a_s] = -\frac{2}{\hbar} \mathrm{Im} \int \mathrm{d}\boldsymbol{r} j(\boldsymbol{r}) \cdot \boldsymbol{A}^*(\boldsymbol{r}, t) \tag{5}$$

Therefore, the heterodyne-detected signal is

$$S(\Gamma) = -\frac{2}{\hbar} \mathrm{Im} \int \mathrm{d}\boldsymbol{r} \mathrm{d}t \langle \boldsymbol{j}(\boldsymbol{r}, t) \cdot \boldsymbol{A}^*(\boldsymbol{r}, t) \rangle \tag{6}$$

The heterodyne-detected signal for Fig. S1 corresponds to

$$\begin{aligned} S(\Gamma) = -\frac{2}{\hbar} \mathrm{Im} \int & \mathrm{d}\boldsymbol{r} \mathrm{d}t \mathrm{d}\boldsymbol{r}_3 \mathrm{d}t_3 \mathrm{d}\boldsymbol{r}_2 \mathrm{d}t_2 \mathrm{d}\boldsymbol{r}_1 \mathrm{d}t_1 (-\frac{i}{\hbar})^3 \\ & \langle \boldsymbol{j}_{\text{left}}(\boldsymbol{r}, t) \boldsymbol{j}_{\text{left}}^\dagger(\boldsymbol{r}_3, t_3) \boldsymbol{j}_{\text{right}}^\dagger(\boldsymbol{r}_2, t_2) \boldsymbol{j}_{\text{right}}(\boldsymbol{r}_1, t_1) \rangle \boldsymbol{A}_s^*(\boldsymbol{r}, t) \boldsymbol{A}_s(\boldsymbol{r}_3, t_3) \boldsymbol{A}_{\text{pu}}(\boldsymbol{r}_2, t_2) \boldsymbol{A}_{\text{pu}}^*(\boldsymbol{r}_1, t_1) \end{aligned} \tag{7}$$

The $\boldsymbol{A}_s$ and $\boldsymbol{A}_{\text{pu}}$ is the vector potential of a probe and pump pulse respectively. The subscript left and right indicates the Liouville space superoperators defined by $O_{\text{left}}\rho = O\rho$ and $O_{\text{right}}\rho = \rho O$. Upon expanding to first order in the probe and taking the difference between left and right polarization of the probe, we get

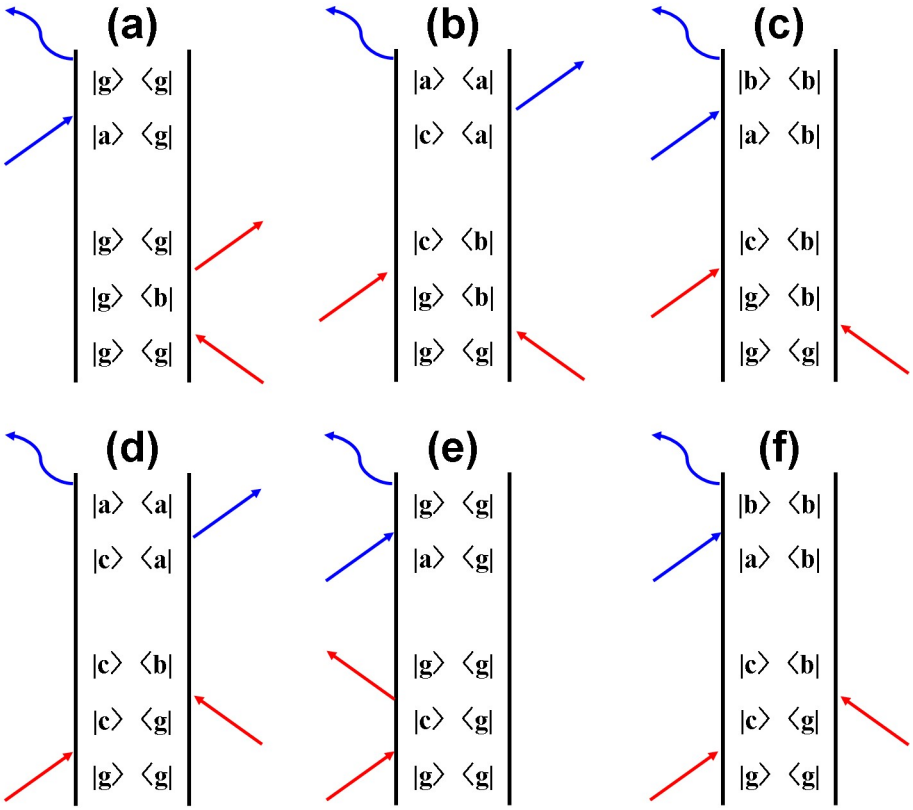

Figure. S 1: Possible pump-probe ladder diagrams. t_1, t_2, and t_3 refer to the time interval between interaction. Red and blue arrow indicates UV pump and X-ray probe interaction, respectively.

$$
\begin{aligned}
S_{jj}(\Gamma) &= -\frac{2}{\hbar}\mathrm{Im}\int \mathrm{d}\boldsymbol{r}t\mathrm{d}\boldsymbol{r}_1\mathrm{d}t_1(-\frac{i}{\hbar})\Big[\langle \boldsymbol{j}_{\mathrm{left}}(\boldsymbol{r},t)\boldsymbol{j}^{\dagger}_{\mathrm{left}}(\boldsymbol{r}_1,t-t_1)\rangle \boldsymbol{A}^*_s(\boldsymbol{r},t)\boldsymbol{A}_s(\boldsymbol{r}_1,t-t_1) \\
&- \langle \boldsymbol{j}_{\mathrm{left}}(\boldsymbol{r},t)\boldsymbol{j}^{\dagger}_{\mathrm{right}}(\boldsymbol{r}_1,t-t_1)\rangle \boldsymbol{A}^*_s(\boldsymbol{r},t)\boldsymbol{A}_s(\boldsymbol{r}_1,t-t_1)\Big] \\
&= \frac{2}{\hbar^2}\mathrm{Re}\int \mathrm{d}\boldsymbol{r}t\mathrm{d}\boldsymbol{r}_1\mathrm{d}t_1\Big[\langle\langle \boldsymbol{j}(\boldsymbol{r})|\mathcal{G}(t_1)\boldsymbol{j}^{\dagger}_{\mathrm{left}}(\boldsymbol{r}_1)|\rho(t-t_1)\rangle\rangle \boldsymbol{A}^*_s(\boldsymbol{r},t)\boldsymbol{A}_s(\boldsymbol{r}_1,t-t_1) \\
&- \langle\langle \boldsymbol{j}(\boldsymbol{r})|\mathcal{G}(t_1)\boldsymbol{j}^{\dagger}_{\mathrm{right}}(\boldsymbol{r}_1)|\rho(t-t_1)\rangle\rangle \boldsymbol{A}^*_s(\boldsymbol{r},t)\boldsymbol{A}_s(\boldsymbol{r}_1,t-t_1)\Big] \\
&= \frac{2}{\hbar^2}\mathrm{Re}\int \mathrm{d}\boldsymbol{r}t\mathrm{d}\boldsymbol{r}_1\mathrm{d}t_1\Big[\langle\langle \boldsymbol{j}(\boldsymbol{r})|\mathcal{G}(t_1)\boldsymbol{j}^{\dagger}_{\mathrm{left}}(\boldsymbol{r}_1)|\rho(t-t_1)\rangle\rangle \\
&- \langle\langle \boldsymbol{j}(\boldsymbol{r})|\mathcal{G}(t_1)\boldsymbol{j}^{\dagger}_{\mathrm{right}}(\boldsymbol{r}_1)|\rho(t-t_1)\rangle\rangle\Big](\boldsymbol{\varepsilon}^*_L\boldsymbol{\varepsilon}_L - \frac{}{3}\boldsymbol{\varepsilon}^*_R\boldsymbol{\varepsilon}_R)\boldsymbol{A}^*_s(\boldsymbol{r},t)\boldsymbol{A}_s(\boldsymbol{r}_1,t-t_1)e^{-i\boldsymbol{k}_s\boldsymbol{r}+i\boldsymbol{k}_s\boldsymbol{r}_1}e^{i\omega_s t_1}
\end{aligned}
\tag{8}
$$

Using that $\varepsilon_L^{a*}\varepsilon_L^b - \varepsilon_R^{a*}\varepsilon_R^b = (-i)\varepsilon_{abz}$, where ε_{abz} is a Levi-Civita symbol and summing over electronic eigenstates, we get

$$\begin{aligned} S_{\mathrm{CD}} = \frac{2}{\hbar^2}\mathrm{Im}\int \mathrm{d}\boldsymbol{r}\mathrm{d}t\mathrm{d}\boldsymbol{r}_1\mathrm{d}t_1\varepsilon_{abz}[\langle\langle j^a(\boldsymbol{r})|\mathcal{G}(t_1)j^{\dagger b}_{\mathrm{left}}(\boldsymbol{r}_1)|\rho(t-t_1)\rangle\rangle \\ - \langle\langle j^a(\boldsymbol{r})|\mathcal{G}(t_1)j^{\dagger b}_{\mathrm{right}}(\boldsymbol{r}_1)|\rho(t-t_1)\rangle\rangle]A_s^*(\boldsymbol{r},t)A_s(\boldsymbol{r}_1,t-t_1)e^{-i\boldsymbol{k}_s\boldsymbol{r}+i\boldsymbol{k}_s\boldsymbol{r}_1}e^{i\omega_s t_1} \end{aligned} \tag{9}$$

and

$$\langle\langle ab|\boldsymbol{j}_L - \boldsymbol{j}_R|cd\rangle\rangle = \boldsymbol{j}_{ac}\delta_{bd} - \boldsymbol{j}_{bd}\delta_{ac} \tag{10}$$

then,

$$\begin{aligned} S_{\mathrm{CD}} &= \frac{2}{\hbar^2}\mathrm{Im}\int \mathrm{d}\boldsymbol{r}\mathrm{d}t\mathrm{d}\boldsymbol{r}_1\mathrm{d}t_1[\langle\langle \boldsymbol{j}(\boldsymbol{r})\times|\mathcal{G}(t_1)\boldsymbol{j}^{\dagger}_{-}(\boldsymbol{r}_1)|\rho(t-t_1)\rangle\rangle]A_s^*(\boldsymbol{r},t)A_s(\boldsymbol{r}_1,t-t_1)e^{-i\boldsymbol{k}_s\boldsymbol{r}+i\boldsymbol{k}_s\boldsymbol{r}_1}e^{i\omega_s t_1} \\ &= \frac{2}{\hbar^2}\mathrm{Im}\int \mathrm{d}t\mathrm{d}t_1[\langle\langle \boldsymbol{j}(\boldsymbol{k}_s)\times|\mathcal{G}(t_1)\boldsymbol{j}^{\dagger}_{-}(-\boldsymbol{k}_s)|\rho(t-t_1)\rangle\rangle]A_s^*(t)A_s(t-t_1)e^{i\omega_s t_1} \\ &= \frac{2}{\hbar^2}\mathrm{Im}\sum_{abc}\int \mathrm{d}t\mathrm{d}t_1(\boldsymbol{j}_{ba}(\boldsymbol{k}_s)\times)e^{-i\omega_{ab}t_1-\Gamma_{ab}t_1}[\boldsymbol{j}^{\dagger}_{ac}(-\boldsymbol{k}_s)\delta_{bd} - \boldsymbol{j}^{\dagger}_{bd}(-\boldsymbol{k}_s)\delta_{ac}]\rho_{cd}(t-t_1)A_s^*(t)A_s(t-t_1)e^{i\omega_s t_1} \end{aligned} \tag{11}$$

where $\boldsymbol{j}_-$ denotes the Liouville space current density superoperator defined by $\boldsymbol{j}_-\rho = \boldsymbol{j}\rho - \rho\boldsymbol{j}$.

$$\begin{aligned} S_{\mathrm{CD}} = \frac{2}{\hbar^2}\mathrm{Im}\sum_{abc}\int \mathrm{d}t\mathrm{d}t_1[\boldsymbol{j}_{ba}(\boldsymbol{k}_s)\times\boldsymbol{j}^{\dagger}_{ac}(-\boldsymbol{k}_s)e^{i(\omega_s-\omega_{ab})t_1-\Gamma_{ab}t_1}\rho_{cb}(t-t_1) \\ - \boldsymbol{j}_{ba}(\boldsymbol{k}_s)\times\boldsymbol{j}^{\dagger}_{bc}(-\boldsymbol{k}_s)e^{i(\omega_s-\omega_{ab})t_1-\Gamma_{ab}t_1}\rho_{ac}(t-t_1)]A_s^*(t)A_s(t-t_1) \end{aligned} \tag{12}$$

Rearranging the sums to factorized out the density matrix after the pump, we get

$$\begin{aligned} S_{\mathrm{CD}}(\boldsymbol{k}_s,\omega_s) = \frac{2}{\hbar^2}\mathrm{Im}\sum_{abc}\int \mathrm{d}t\mathrm{d}t_1 A_s^*(t)A_s(t-t_1)\rho_{cb}(t-t_1) \\ [\boldsymbol{j}_{ba}(\boldsymbol{k}_s)\times\boldsymbol{j}^{\dagger}_{ac}(-\boldsymbol{k}_s)e^{i(\omega_s-\omega_{ab})t_1-\Gamma_{ab}t_1} - \boldsymbol{j}_{ac}(\boldsymbol{k}_s)\times\boldsymbol{j}^{\dagger}_{ab}(-\boldsymbol{k}_s)e^{i(\omega_s-\omega_{ca})t_1-\Gamma_{ca}t_1}] \end{aligned} \tag{13}$$

In the impulsive limit, $A_s(t) = \delta(t-T)A_s$, $A_s(t-t_1) = \delta(t-t_1-T)A_s$, where $t \to T$, and $t_1 \to 0$.

We now express explicitly $\rho_{cb}(T)$. At second order in the pump interaction (Fig S4), we have

$$\begin{aligned} \rho_{cb}(T) &= \langle\langle cb|\rho(T)\rangle\rangle \\ &= -(\frac{-i}{\hbar})^2\int \mathrm{d}\boldsymbol{r}_1\mathrm{d}\boldsymbol{r}_2\mathrm{d}t_1\mathrm{d}t_2\langle\langle cb|\boldsymbol{j}_-(\boldsymbol{r}_2,t_2)\boldsymbol{j}_-(\boldsymbol{r}_1,t_1)|\rho(T-t_1-t_2)\rangle\rangle A^*_{\mathrm{pu}}(\boldsymbol{r}_2,T-t_2)A_{\mathrm{pu}}(\boldsymbol{r}_1,T-t_2-t_1) \\ &= -(\frac{-i}{\hbar})^2\int \mathrm{d}\boldsymbol{r}_1\mathrm{d}\boldsymbol{r}_2\mathrm{d}t_1\mathrm{d}t_2\Big(\langle\langle cb|\mathcal{G}(t_2)\boldsymbol{j}_{\mathrm{right}}(\boldsymbol{r}_2)\mathcal{G}(t_1)\boldsymbol{j}^{\dagger}_{\mathrm{left}}(\boldsymbol{r}_1)|\rho(t_0)\rangle\rangle A^*_{\mathrm{pu}}(\boldsymbol{r}_2,T-t_2)A_{\mathrm{pu}}(\boldsymbol{r}_1,T-t_2-t_1) \\ &\quad + \langle\langle cb|\mathcal{G}(t_2)\boldsymbol{j}^{\dagger}_{\mathrm{left}}(\boldsymbol{r}_2)\mathcal{G}(t_1)\boldsymbol{j}_{\mathrm{right}}(\boldsymbol{r}_1)|\rho(t_0)\rangle\rangle A_{\mathrm{pu}}(\boldsymbol{r}_2,T-t_2)A^*_{\mathrm{pu}}(\boldsymbol{r}_1,T-t_2-t_1)\Big) \end{aligned} \tag{14}$$

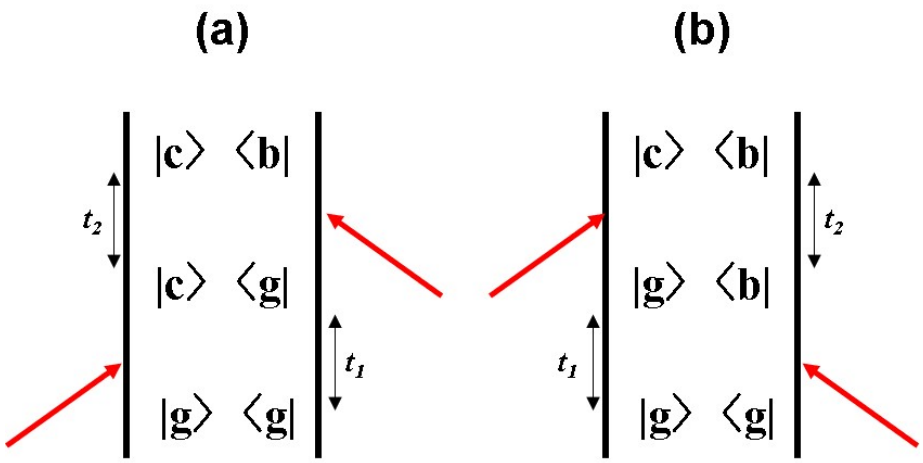

Figure. S 2: Ladder diagrams for pump interaction. t_1 and t_2, refer to the time interval between two pump interactions.

Since, $\rho(t_0) = |gg\rangle\rangle$

$$\rho_{cb}(T) = (\frac{1}{\hbar})^2 \int \mathrm{d}\boldsymbol{r}_1 \mathrm{d}\boldsymbol{r}_2 \mathrm{d}t_1 \mathrm{d}t_2 \Big(\mathcal{G}_{cb,cb}(t_2) \boldsymbol{j}_{bg}(\boldsymbol{r}_2) \mathcal{G}_{cg,cg}(t_1) \boldsymbol{j}^{\dagger}_{cg}(\boldsymbol{r}_1) \boldsymbol{A}^{*}_{\mathrm{pu}}(\boldsymbol{r}_2, T - t_2) \boldsymbol{A}_{\mathrm{pu}}(\boldsymbol{r}_1, T - t_2 - t_1)$$

$$+ \mathcal{G}_{cb,cb}(t_2) \boldsymbol{j}^{\dagger}_{cg}(\boldsymbol{r}_2) \mathcal{G}_{gb,gb}(t_1) \boldsymbol{j}_{bg}(\boldsymbol{r}_1) \boldsymbol{A}_{\mathrm{pu}}(\boldsymbol{r}_2, T - t_2) \boldsymbol{A}^{*}_{\mathrm{pu}}(\boldsymbol{r}_1, T - t_2 - t_1) \Big)$$

$$= \frac{1}{\hbar^2} \int \mathrm{d}t_1 \mathrm{d}t_2 \Big(e^{-i\omega_{cb}t_2 - \Gamma_{cb}t_2} e^{-i\omega_{cg}t_1 - \Gamma_{cg}t_1} \boldsymbol{j}_{bg}(\boldsymbol{k}_{\mathrm{pu}}) \boldsymbol{j}^{\dagger}_{cg}(-\boldsymbol{k}_{\mathrm{pu}}) \boldsymbol{A}^{*}_{\mathrm{pu}}(T - t_2) \boldsymbol{A}_{\mathrm{pu}}(T - t_2 - t_1)$$

$$+ e^{-i\omega_{cb}t_2 - \Gamma_{cb}t_2} e^{-i\omega_{gb}t_1 - \Gamma_{gb}t_1} \boldsymbol{j}^{\dagger}_{cg}(-\boldsymbol{k}_{\mathrm{pu}}) \boldsymbol{j}_{bg}(\boldsymbol{k}_{\mathrm{pu}}) \boldsymbol{A}_{\mathrm{pu}}(T - t_2) \boldsymbol{A}^{*}_{\mathrm{pu}}(T - t_2 - t_1) \Big) \quad (15)$$

In the impulsive limit, $\boldsymbol{A}_{\mathrm{pu}}(t) = \delta(t)\boldsymbol{A}_{\mathrm{pu}}$, where $t_2 \to T$, and $t_1 \to 0$. The Fourier transform of pump pulse in time-domain to frequency domain gives,

$$\boldsymbol{A}_{\mathrm{pu}}(T - t_1) = \int \frac{\mathrm{d}\omega_1}{2\pi} \boldsymbol{A}_{\mathrm{pu}}(\omega_1) e^{-i\omega(T - t_1)} \quad (16)$$

and

$$\int_0^{\infty} \mathrm{d}t_2 e^{i(\omega_1 - \omega_2 - \omega_{cb}t_2 - \Gamma_{cb}t_2} = \frac{i}{\omega_1 - \omega_2 - \omega_{cb} + i\Gamma_{cb}} \quad (17)$$

Hence, the density matrix at waiting time T becomes,

$$\rho_{cb}(T) = -\frac{1}{\hbar^2}\int \frac{\mathrm{d}\omega_1}{2\pi}\frac{\mathrm{d}\omega_2}{2\pi}\boldsymbol{A}_{\mathrm{pu}}(\omega_1)\boldsymbol{A}_{\mathrm{pu}}(\omega_2) \\ \left[\frac{\boldsymbol{j}_{bg}(\boldsymbol{k}_{\mathrm{pu}})\cdot\varepsilon^*_{\mathrm{pu}}\cdot\boldsymbol{j}^\dagger_{cg}(-\boldsymbol{k}_{\mathrm{pu}})\cdot\varepsilon_{\mathrm{pu}}e^{i(\omega_2-\omega_1)T}}{(\omega_1-\omega_2-\omega_{cb}+i\Gamma_{cb})(\omega_1-\omega_{cg}+i\Gamma_{cg})} + \frac{\boldsymbol{j}^\dagger_{cg}(-\boldsymbol{k}_{\mathrm{pu}})\cdot\varepsilon_{\mathrm{pu}}\cdot\boldsymbol{j}_{bg}(\boldsymbol{k}_{\mathrm{pu}})\cdot\varepsilon^*_{\mathrm{pu}}e^{-i(\omega_2-\omega_1)T}}{(-\omega_1+\omega_2-\omega_{cb}+i\Gamma_{cb})(-\omega_1-\omega_{gb}+i\Gamma_{gb})}\right] \tag{18}$$

Likewise, the final TRCD signal becomes,

$$S_{\mathrm{CD}}(\omega_s,T) = \frac{2}{\hbar^2}\frac{1}{(2\pi)^2}N\mathrm{Re}\sum_{abc}\boldsymbol{A}^*_s(\omega_s)\boldsymbol{A}_s(\omega_s)\rho_{cb}(T) \\ \left[\frac{\boldsymbol{j}_{ba}(\boldsymbol{k}_s)\times\boldsymbol{j}^\dagger_{ac}(-\boldsymbol{k}_s)}{\omega_s-\omega_{ab}+i\Gamma_{ab}} - \frac{\boldsymbol{j}_{ac}(\boldsymbol{k}_s)\times\boldsymbol{j}^\dagger_{ab}(-\boldsymbol{k}_s)}{-\omega_s-\omega_{ca}+i\Gamma_{ca}}\right] \tag{19}$$

Finally, substituting a, b, and c into c, e', and e, respectively, gives the final expression in the manuscript.

2 Quantum simulation results

We compared our quantum calculations with previous work of Rubio [1] which performed CASSCF calculations within the same active space (13o/18e) for the electronic structure calculation of the Mg-porphyrin. To that end, we computed transition energies (Table S1 and S2) and transition dipole moment (Fig. S3) of the Mg-porphyrin calculated at the CASSCF (13o/18e) level with C_1 and D_{2h} symmetry option (note that the highest symmetry option in MOLPRO is D_{2h}). By comparing the orbital configuration of each excited state of the active orbitals, we assigned our e_1, e_3, e_5, and e_7 states to e_1 to e_4 states (Q band to N band) of Rubio's work and those of D_{2h} symmetry. The e_1, e_3, e_5, and e_7 states are originally doubly degenerate, however, they might split into several non-degenerate states due to the loss of symmetry [1, 2]: for example, the Q bands split into e_1 and e_2 states. Discrepancies of the computed transition energies compared to experimental data are due to the lack of dynamics correlation in CASSCF. However, our computation matches the results of the CASSCF calculation of Rubio [1] in terms of transition energies and orbital configurations. Moreover, the square of transition dipole moment with D_{2h} symmetry shows the same trend ($e_1 < e_3, e_3 > e_5$, and $e_5 < e_7$). The small deviation from Rubio's work mainly originates from the different basis set and since the oscillator strength was calculated with CASPT2 in that study. It is also consistent with experiment that the absorption of e_1 is very weak and e_3 shows the most intense absorption [3].

	CASSCF (13o/20e) with C_1 symmetry				Rubio's work[5]: CASSCF (13o/18e)			Experiment[1]
	Transition Energy	Square of the transition dipole moment, μ^2	Transition dipole moment direction	Main orbital configuration (with D_{2h} notation)	Transition Energy	Oscillator Strength	Main orbital configuration (D_{4h})	Transition Energy
e_1	3.125	0.199	x	$6B_{1u} \rightarrow 4B_{2g}$ (B_{3u}) $2A_u \rightarrow 4B_{3g}$ (B_{3u})	3.05	0.008	$4a_{2u} \rightarrow 4e_g$ $1a_{1u} \rightarrow 4e_g$	2.14
e_2	3.157	0.748	y	$6B_{1u} \rightarrow 4B_{3g}$ (B_{2u}) $2A_u \rightarrow 4B_{2g}$ (B_{2u})				
e_3	5.051	14.054	x	$6B_{1u} \rightarrow 4B_{2g}$ (B_{3u}) $2A_u \rightarrow 4B_{3g}$ (B_{3u}) $4B_{1u} \rightarrow 4B_{2g}$ (B_{3u})	4.95	0.923	$4a_{2u} \rightarrow 4e_g$ $1a_{1u} \rightarrow 4e_g$ $3a_{2u} \rightarrow 4e_g$	3.18
e_4	5.274	0.000	y	$3B_{3g} \rightarrow 4B_{2g}$ (B_{1g})				
e_5	5.400	20.418	y	$6B_{1u} \rightarrow 4B_{3g}$ (B_{2u}) $2A_u \rightarrow 4B_{2g}$ (B_{2u})	5.28	0.200	$2b_{2u} \rightarrow 4e_g$	3.40
e_6	5.492	0.000	x	$3B_{2g} \rightarrow 4B_{2g}$ (A_g)				
e_7	5.527	6.413	x	$4B_{1u} \rightarrow 4B_{2g}$ (B_{3u})	5.83	0.379	$3a_{2u} \rightarrow 4e_g$	3.81
e_8	5.664	0.000	y	$3B_{2g} \rightarrow 4B_{3g}$ (B_{1g})				
e_9	5.793	0.000	x	$3B_{3g} \rightarrow 4B_{3g}$ (A_g)				

Table S 1: Comparison of transition energies (eV), transition dipole moment (a.u.), main orbital configuration of Mg-porphyrin between this study (with C_1 symmetry), Rubio's work [1] and experimental results [3]. The main orbital configuration of C_1 symmetry was converted to the orbital notations of D_{2h} symmetry for convenience.

	CASSCF (13o/20e) with D_{2h} symmetry				Rubio's work[5]: CASSCF (13o/18e)			Experiment[1]
	Transition Energy	Square of the transition dipole moment, μ^2	Transition dipole moment direction	Main orbital configuration (Wavefunction symmetry)	Transition Energy	Oscillator Strength	Main orbital configuration	Transition Energy
e_1	2.869	0.493	x	$2A_u \rightarrow 4B_{3g}(B_{3u})$ $6B_{1u} \rightarrow 4B_{2g}(B_{3u})$	3.05	0.008	$4a_{2u} \rightarrow 4e_g$ $1a_{1u} \rightarrow 4e_g$	2.14
e_1'	2.869	0.493	y	$2A_u \rightarrow 4B_{2g}(B_{2u})$ $6B_{1u} \rightarrow 4B_{3g}(B_{2u})$				
e_2	4.836	16.945	x	$6B_{1u} \rightarrow 4B_{2g}(B_{3u})$ $2A_u \rightarrow 4B_{3g}(B_{3u})$ $4B_{1u} \rightarrow 4B_{2g}(B_{3u})$	4.95	0.923	$4a_{2u} \rightarrow 4e_g$ $1a_{1u} \rightarrow 4e_g$ $3a_{2u} \rightarrow 4e_g$	3.18
e_2'	4.836	16.945	y	$6B_{1u} \rightarrow 4B_{3g}(B_{2u})$ $2A_u \rightarrow 4B_{2g}(B_{2u})$ $4B_{1u} \rightarrow 4B_{3g}(B_{2u})$				
e_3	5.281	1.417	x	$5B_{1u} \rightarrow 4B_{2g}(B_{3u})$	5.28	0.200	$2b_{2u} \rightarrow 4e_g$	3.40
e_3'	5.281	1.417	y	$5B_{1u} \rightarrow 4B_{3g}(B_{2u})$				
e_4	5.815	2.521	x	$4B_{1u} \rightarrow 4B_{2g}(B_{3u})$	5.83	0.379	$3a_{2u} \rightarrow 4e_g$	3.81
e_4'	5.815	2.521	y	$4B_{1u} \rightarrow 4B_{3g}(B_{2u})$				

Table S 2: Comparison of transition energies (eV), transition dipole moment (a.u.), main orbital configuration of Mg-porphyrin between this study (with D_{2h} symmetry), Rubio's work [1] and experimental results [3].

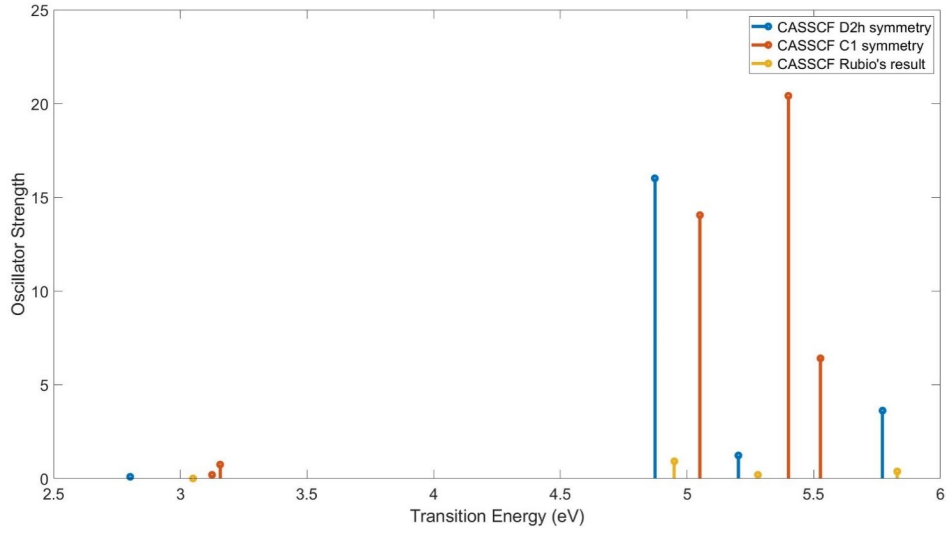

Figure. S 3: Stick spectra of the oscillator strength for the valence excitations from the ground state. Blue: CASSCF calculation with D_{2h} symmetry, Red: CASSCF calculation with C_1 symmetry, Yellow: CASSCF result [1].

3 Time-dependent density matrix elements and Average transition current density

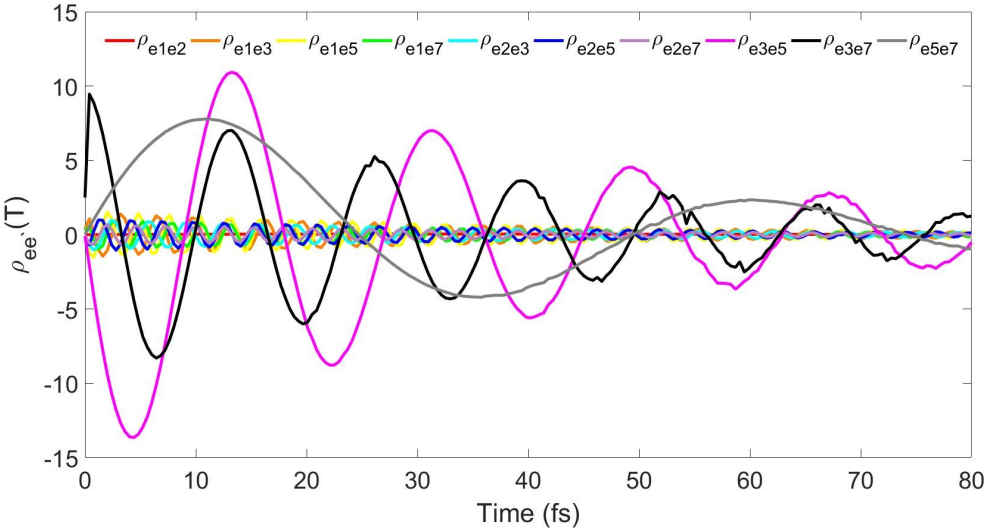

Figure. S 4: The time-dependent density matrix for various coherences of valence excited states. The density matrix originating only from e_1, e_2, e_3, e_5, and e_7 are shown.

j_{ab}	c_1		c_2	
	x	y	x	y
e_3	-7.137	2.086	-7.137	2.087
e_5	-0.300	-4.448	-0.300	-4.448
e_7	0.245	-5.231	0.245	-5.231

Table S 3: The average transition current density value for the transition from e_3, e_5, and e_7 valence state to c_1 and c_2 core states in the real space (x and y component are separately shown, Unit: 10^{-7} e/bohr^3), where e is the electron charge.

References

[1] M. Rubio, B. O. Roos, L. Serrano-Andrés and M. Merchán, J. Chem. Phys., 1999, **110**, 7202-7209.

[2] D. Sundholm, Chem. Phys. Lett., 2000, **317**, 392-399.

[3] G. D. Dorough, J. R. Miller and F. M. Huennekens, J. Am. Chem. Soc., 1951, **73**, 4315-4320.